Mining, Metallurgy & Exploration (2023) 40:263–276
https://doi.org/10.1007/s42461-022-00720-y

Numerical Simulation Study on Mechanism of Roof Directional Breaking in Gob-Side Entry Formed Automatically Without Coal Pillars

Jun Zhang[1,2] · Yajun Wang[2,3] · Manchao He[1,2] · Chengzhang Gao[4] · Ben Liu[1,2] · Shilin Hou[1,2] · Gang Yang[1,2] · Jianning Liu[1,2] · Jun Yang[1,2] · Yayun Li[4]

Received: 16 March 2022 / Accepted: 15 December 2022 / Published online: 22 December 2022

Abstract
To explore the mechanism of roof directional breaking in gob-side entry formed automatically without coal pillars, the numerical simulation was used to study the deformation movement of roof, the deformation evolution of roadway, and the stress distribution of roadway under roof directional breaking and non-roof directional breaking. Based on the results, the deformation movement of roof is divided into three stages: the goaf roof collapse stage, the basic roof deformation stage, and the basic roof stability stage. The goaf is filled with gangue due to the broken expansion characteristics of the collapsed rock under the roof directional breaking. Due to the supporting force of gangue, the deformation of the basic roof under the roof directional breaking is smaller than that under the non-roof directional breaking, which reduces the influence of the deformation of the basic roof on the deformation of the roadway roof and improves the integrity of the roadway. At the same time, roof directional breaking cuts off the stress transfer path of partial roof, which weakens the peak stress convergence on the arc side, transfers the peak stress convergence to deeper, and improves the stability of roadway. Finally, a field test was carried out to further verify the accuracy of the numerical simulation. The field test results are in good agreement with the numerical simulation results. The roadway deformation is small and meets the requirements of safety production. It is proved that roof directional breaking plays a positive role in improving the stability of the roadway.

Keywords Roof directional breaking · Gob-side entry retaining · Roof movement · Deformation evolution · Stress distribution

1 Introduction

Longwall mining has made an enormous contribution to underground coal mining in the world [1–4]. In the process of longwall mining, a coal pillar is usually needed between adjacent working faces to protect the roadway in the next working face. With the continuous mining, the overlying rock on the working face continues to rotate, deform, and collapse, which will not only causes strong mine pressure on the working face [5–7] but also causes the stress convergence of the remaining coal pillars [8–10], and ultimately leads to spalling of the roadway side and destruction of the roadway roof [11, 12]. At the same time, the remaining coal pillars will also cause waste of resources. For example, the strike length of longwall mining plate in Svea Nord Mine is 2500 m, and the height of mining is 4 m [13]. The width of the remaining coal pillar between adjacent working faces is 40 m, which means that each mining face will lead to about 600,000 tons of coal resources waste.

To avoid the waste of coal resources caused by remaining coal pillars, it is proposed to use a filling body instead of coal pillars, such as gangue filling [14] and concrete filling [15]. Although this method increases the recovery rate of resources, the stress convergence still exists in the position of filling body, which greatly reduces the safety

✉ Yajun Wang
yyajun1990@163.com

1 School of Mechanics and Civil Engineering, China University of Mining & Technology, Beijing, Beijing 100083, China

2 State Key Laboratory for Geomechanics & Deep Underground Engineering, China University of Mining & Technology, Beijing, Beijing 100083, China

3 School of Civil and Resource Engineering, University of Science and Technology, Beijing, Beijing 100083, China

4 ShanXiYinFeng Science & Technology CO. LTD, Taiyuan 030000, China

and stability of roadway. In order to further solve the safety problem of roadway, the author's research team [16, 17] proposed a technology of gob-side entry formed automatically without coal pillars (GEFAWCP) based on roof directional breaking (RDB). The RDB fundamentally changes the roof structure, and the stress distribution of roadway was optimized. One side of the roadway is formed by collapsed rock and the other by solid coal, which automatically form the roadway behind the working face. The support of goaf gangue reduces the rotation deformation of basic roof, which reduces the stress convergence and deformation of roadway and improves the stability of roadway.

Since then, many scholars have adopted different methods to study the deformation movement of roof, the deformation evolution of roadway, and the stress distribution of roadway under RDB. Wang et al. [18, 19] analyzed the distribution and evolution of mining stress during RDB and roadway retaining through similar simulation experiments and revealed the control mechanism of roadway under the action of RDB. Yang et al. [20–22] analyzed the influence of different fracture positions of the basic roof on the support and deformation of the roadway. By using the RDB to change the fracture position of the basic roof, the safety of the roadway is ensured. The mechanical analysis of the stress and deformation of the roadway during RDB and retaining was carried out, and the control countermeasures of roadway deformation were put forward. Wang et al. [23] used Mohr–Coulomb theory to analyze the stress state and variation characteristics of roadway during gob-side entry retaining and proposed the effective control countermeasures. Gao et al. [24] analyzed the rock pressure law of gob-side entry retaining under the influence of faults and put forward the corresponding control technology. Compared with the traditional fault crossing, the deformation of surrounding rock was decreased and effectively controlled. Liu et al. [25, 26] studied the rock fragmentation effect under the action of RDB and analyzed the control mechanism of rock-broken expansion coefficient on the stability of key rock blocks. Yang et al. [27] studied that the destruction of roadway is mainly caused by local tensile stress without support; therefore, an active flexible support method is proposed to improve the tensile stress state of roadway, and the field application results show that the support technology is feasible. Zhang et al. [28, 29] studied the movement process of roof strata under RDB and designed the parameters of RDB. The results showed that reasonable RDB parameters could be effective.

Through the study of previous scholars, it can be known that the roof rock above the goaf can be collapsed by RDB, and then the rock-broken expansion characteristics are used to support the goaf roof, which reduces the influence of roof deformation of goaf on the deformation of roadway roof, optimizes the stress distribution of roadway, and finally improves the stability of roadway. However, previous studies mainly focused on the deformation of roadway and the stress characteristics of supporting structure. These data can be obtained through field monitoring. Few scholars pay attention to the caving of gangue in goaf and the roof movement process under gangue support, because these results are not easy to be monitored on site. Therefore, the scope of this study is to analyze and simulate the roof deformation process under the conditions of roof directional breaking and non-roof directional breaking (NRDB), and to clarify the influence of roof strata movement at different stages on the deformation and stress distribution characteristics of roadway. The objective of this study is to identify the mechanism of DRB for GEFAWCP. Finally, field test verification is essential to verify the accuracy of numerical simulation, because the most effective way to verify the accuracy of numerical simulation is to prove it in the field test.

2 Engineering Background

2.1 Project Summary

Ningtiaota coal mine produces 18 million tons of coal annually and is located in Shaanxi Province, China. There are 7 stable coal seams that can be mined. At present, the main coal seam is 2^{-2}# coal, with an average thickness of 4.11 m and burial depth of 115–170 m. The test working face is S1201-II working face with a length of 280 m and a strike length of 2344 m, and the layout of S1201-II working face is shown in Fig. 1a. The automatically formed roadway is the ventilation roadway of the working face, and another roadway in working face is formed in advance excavation. Lithology and thickness of roof and floor are shown in Fig. 1b.

2.2 Technical Process of GEFAWCP

To better study the mechanism of RDB, it is necessary to understand the technical process of GEFAWCP. In this technique, the roadway on one side of the working face is automatically formed during mining. As shown in Fig. 2a, the roadway is formed by the cutting of the shearer. The drum of the shearer is circular; therefore, the shape of the side near the solid coal of the roadway is arc, which is called the arc side. As shown in Fig. 2b, after the roadway is formed, the shearer is far away from the roadway and mining at the working face. Because the working face is long, the shearer needs to work in the working face for a period, and there is enough time to support the roadway during this time. The roadway roof is supported by high pre-tightening force anchor cable, and the arc side is supported by anchor bolt. As shown in Fig. 2c, after the support of the roof and the arc

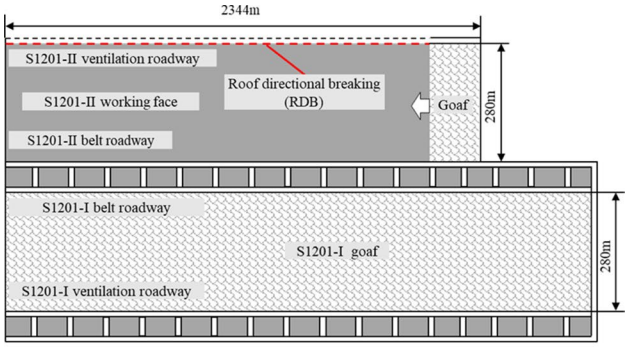

(a) the layout of S1201- II working face

Columnar	Lithology	Thickness(m)
	13.23	Medium sandstone
	2.23	Siltstone
	4.11	Coal
	9.58	Siltstone

(b) lithology and thickness of roof and floor

Fig. 1 Engineering conditions of S1201-II working face

side is completed, the RDB is implemented through the roof directional breaking device (RDBD) [30, 31], and support is carried out on the side of the goaf. As shown in Fig. 2d, after the mining of the working face, the roof rock after RDB fall to the goaf to form gangue, and the rock has the characteristics of broken expansion [30]. The roadway is retained by the support of gangue in the goaf and roadway support. The retained roadway can be used during the next working face. Moreover, it is not necessary to place coal pillars between adjacent working faces when using this method.

3 Numerical Modeling

3.1 Modeling

In this paper, the numerical simulation method is used to study the deformation evolution and stress distribution characteristics of roadway in GEFAWCP. In essence, the Universal Distinct Element Code (UDEC) can not only simulate the movement, deformation, and complete stripping of rock strata but also clearly simulate the stress change and transmission. Therefore, the UDEC software was used to analyze the roof movement, deformation evolution law, and stress distribution characteristics of roadway.

A numerical model has been developed based on the geological situation of S1201-II working face. As shown in Fig. 3, the model size is 150 m*60 m, simulating the cross section of longwall face. To eliminate the effects of boundary conditions, the model retains the region with a width of 30 m on the left side of the model. To study the stress distribution characteristics of arc side, the region with a width of 50 m is retained on the right side of the model. The in situ stress measured by the borehole stress method, the vertical stress is 2.5 MPa, and the horizontal stress is 1.25 MPa. Horizontal and vertical displacements of the model are constrained at the lateral and bottom boundary of the model, respectively. Considering that the fracture and collapse behavior of rock strata are mainly dominated by the discontinuous surface in rock mass, the elastic–plastic model is adopted to the complete rock mass and the coulomb slip model is adopted to and the contact surface. Based on the cantilever beam theory, a rectangular block is used to simulate the fracture shape of the collapsed rock mass in this model. The side near the coal body of the roadway is the arc side. Therefore, the trigon model is considered to avoid the severe fluctuation of the stress near the arc side due to the uneven change of the block shape, which affects the stress distribution results.

3.2 Calculation and Validation of Numerical Model Parameters

The physical and mechanical parameters of intact rock in the test working face were obtained by drilling sampling and indoor physical and mechanical tests. There are some cracks and joints in rock mass; so, it is necessary to ignore the intact rock parameters. By obtaining the RQD value of the intact rock, the Young's modulus of the intact rock (E_i) is converted to the Young's modulus of the rock mass (E_m) by using the RQD- E_m/ E_i relationship [31, 32].

$$\frac{E_m}{E_i} = 10^{0.0186RQD-1.91} \tag{1}$$

Then, the unconfined compressive strength of rock mass is obtained by using the relationship between the ratio of unconfined compressive strength (σ_{cm}/σ_{ci}) and the ratio of Young's modulus (E_m/ E_i) [33, 34].

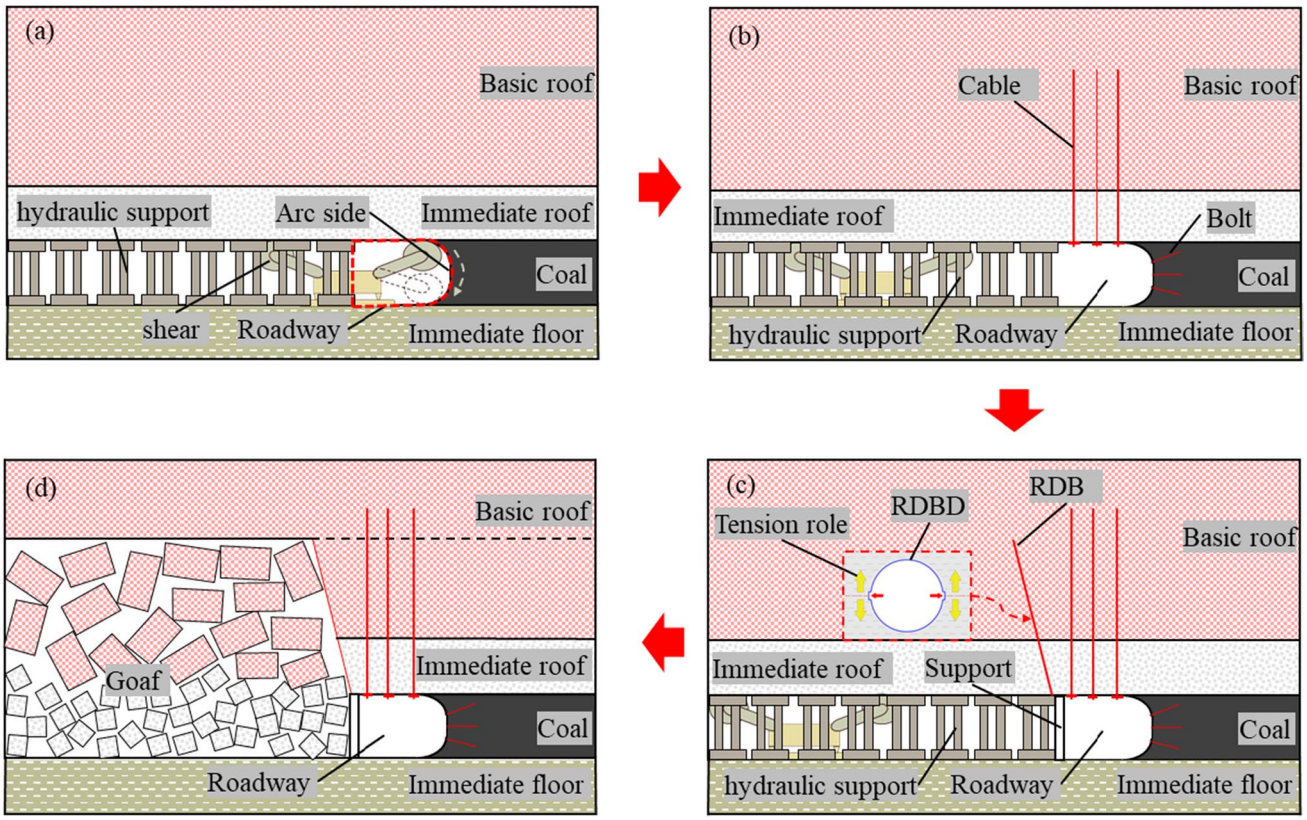

Fig. 2 Technical process of GEFAWCP

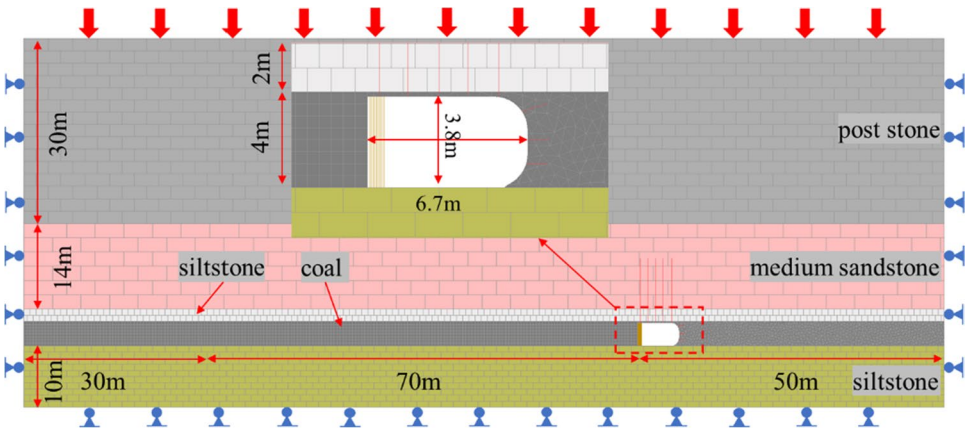

Fig. 3 Numerical simulation model

$$\frac{\sigma_{cm}}{\sigma_{ci}} = \left(\frac{E_{\mathrm{m}}}{E_{\mathrm{i}}}\right)^{\eta} \tag{2}$$

When the failure mode of rock mass cannot be evaluated, the average value of η is 0.63.

As shown in Table 1, the reasonable estimation of tensile strength of rock mass is 1/10 of compressive strength [35].

According to the obtained Young's modulus and the Poisson's ratio (v), the bulk modulus (K) and shear modulus (G) can be calculated by the following formula [36]:

$$K = \frac{E}{3(1-2v)} \tag{3}$$

$$G = \frac{E}{2(1+2v)} \tag{4}$$

Before numerical simulation, the parameters and simulation results of rock should be verified according to the field measured data. This is achieved through unconfined compression tests on numerical samples. The shape and size

Table 1 Physical and mechanical parameters of intact rock and rock mass

Lithology	Density (kg·m^{-3})	Height m	Intact rock		RQD	Rock mass		
			σ_{ci} (MPa)	E_i (GPa)		E_i (GPa)	σ_{cm}(MPa)	σ_{cm}(MPa)
Overlying strata	2000	30	13.13	7.84	74	2.29	6.05	0.61
Medium sandstone	2280	14	22.70	10.16	92	6.43	17.01	1.70
Siltstone2	2040	2	16.26	9.25	83	3.98	9.56	0.96
Coal seam	1260	4	15.30	8.69	82	3.58	8.76	0.88
Siltstone1	2410	10	29.60	19.65	87	10.04	19.38	1.94

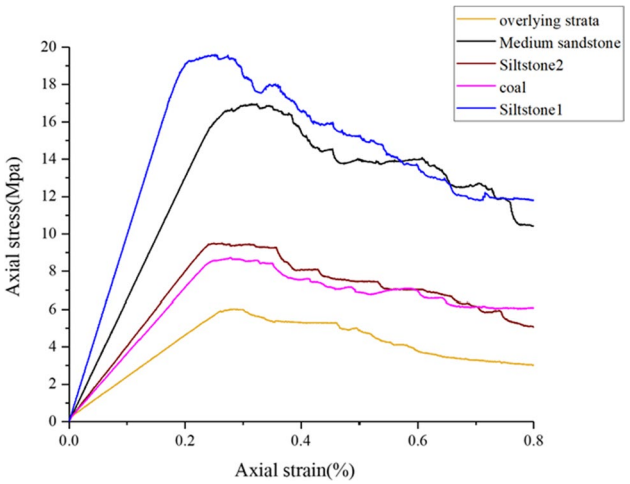

Fig. 4 The axial stress–strain curve of UDEC specimen under unconfined compression

of the calibrated specimen grid are the same as those of the mining model.

The normal stiffness (k_n) and shear stiffness (k_s) of the contact parameters are iteratively calibrated by numerical unconfined compression tests. The loading rate is 0.1 m/s. The calibrated stress–strain curve by UDEC is shown in Fig. 4. The parameters of calibrated rock mass in UDEC are shown in Table 2. The error of calibrated rock mass parameters in UDEC is shown in Table 3.

3.3 Model Support Parameters

The roof of ventilation roadway in the S1201-II working face is supported by five anchor cables with a length of 10.5 m. Hydraulic support is installed on the side near the goaf, and bolt support is used on the side of the arc side. The anchor cable is simulated by the cable element, the bolt support is simulated by the bolt element, and the temporary support is simulated by the support unit. The parameters of anchor cable, bolt support, and temporary support are shown in Table 4.

Table 2 Parameters of calibrated rock mass in UDEC

Lithology	Block parameters			Contact parameters			
	E_m (GPa)	v	k_n (GPa·m^{-1})	K_s (Gpa·m^{-1})	C^j(MPa)	Φ^j (°)	σ_t^j (MPa)
Overlying strata	2.14	0.20	774	310	2.43	40.91	0.76
Medium sandstone	6.63	0.26	1788	715	6.29	41.33	1.32
Siltstone2	4.07	0.23	1236	494	4.48	38.45	0.94
Coal seam	3.73	0.21	1158	463	3.96	39.69	0.89
Siltstone1	10.40	0.28	2313	925	8.6	40.81	1.72

Table 3 Error of calibrated rock mass parameters in UDEC

Lithology	E_m (GPa)			σ_{cm} (MPa)		
	Target	Calibrated	Error (%)	Target	Calibrated	Error (%)
Overlying strata	2.29	2.23	2.6	6.05	6.03	0.3
Medium sandstone	6.43	6.48	0.7	17.01	17.00	0.1
Siltstone2	3.98	2.62	0.8	9.56	9.47	0.3
Coal seam	3.58	3.54	1.1	8.76	8.74	0.2
Siltstone1	10.04	9.98	0.6	19.38	19.61	1.2

Table 4 Support parameters

Type	Parameters	Value
Cable	Density (kg/m^3)	7500
	Elastic modulus (GPa)	200
	Length (m)	10.5
	Diameter (mm)	21.8
	Tensile capacity (KN)	530
	Resin-bonded stiffness (N/m^2)	2×10^9
	Bond Strength (N/m)	4×10^5
	Pre-tightening force (KN)	280
Bolt	Density (kg/m^3)	2100
	Elastic modulus (GPa)	200
	Length (m)	1.6
	Diameter (mm)	18
	Tensile capacity (KN)	300
	Resin-bonded stiffness (N/m^2)	1×10^9
	Bond strength (N/m)	3×10^5
	Pre-tightening force(KN)	50
Support	Axial stiffness (GPa/m)	3
	Height (m)	3.8
	Diameter (mm)	600
	Compressive yield strength (MPa)	40

4 Analysis of Numerical Simulation Results

4.1 Analysis of Roof Deformation Process

The RDB state and NRDB state were simulated and compared. In the RDB state, the height of RDB is 9 m and the angle of RDB is 10°. To simulate the roof deformation movement and the broken expansion characteristics of gangue in the goaf, after the formation of the roadway, 2 m was mined each time along the direction far from the roadway, and 20,000 steps were operated to make the roof rock completely collapse in the goaf. The results of roadway roof deformation are shown in Figs. 5 and 6. To facilitate the analysis, in 0–600,000 steps, the results of roof deformation are recorded every 60,000 steps, and in 600,000–160,000 steps, the results of roof deformation are recorded every 200,000 steps. It should be noted that some operational steps are chosen as the beginning/end of a certain stage to describe the stage of roof deformation more accurately. The point with the maximum deformation of basic roof is selected to record and analyze. The location of the monitoring points is shown in Figs. 5o and 6o.

The basic roof near the roadway side rotates in a cantilever shape, and the point with the maximum deformation of the basic roof represents the rotation deformation degree. For ease of analysis, the deformation coefficient of the basic roof is defined as follows:

$$D = \frac{H}{M}(0 \le H \le M) \tag{5}$$

where M is the height of the mining, and H is the deformation of the basic roof.

The larger deformation of the basic roof, the larger deformation coefficient of the corresponding basic roof. The deformation coefficient monitoring results of the basic roof are shown in Fig. 7.

According to the monitoring results, the deformation movement of roof can be divided into three stages. In the NRDB state, as shown in Fig. 5a–d. In the mining process, the immediate roof continued to collapse, the basic roof did not have any obvious deformation, and the deformation coefficient was almost 0. Therefore, this stage is called the first stage: the goaf roof collapse stage. As shown in Fig. 5d–o, the basic roof begins to rotate and deform. During the deformation of the basic roof, the gangue formed by the collapse of the immediate roof cannot fill the goaf. There is a large space in the goaf, and the angle with large rotation deformation of the basic roof can contact the gangue. When the numerical model runs to Fig. 5n, the rotational deformation of the basic roof touches the gangue in the goaf, then the basic roof slowly reaches a stable state under the support of the gangue, which is called the second stage: the basic roof deformation stage. As shown in Fig. 5n, o, the basic roof reaches a stable state and no longer deformed, and the final deformation coefficient of the basic roof reaches 0.99. The basic roof finally reaches almost the maximum deformation. This stage is called the third stage: the basic roof stability stage.

In the RDB state, as shown in Fig. 6a to c. In the mining process, because of the influence of the RDB, the immediate roof, and part of the basic roof continue to collapse, there is no obvious deformation of the basic roof above the height of RDB, and the deformation coefficient of the basic roof is almost 0. This stage is called the first stage: the goaf roof collapse stage. As shown in Fig. 6c–l, the basic roof above the height of RDB begins to rotate and deform. Due to the effect of RDB and the broken expansion characteristics of rock, the goaf was filled with gangue. The small angle of the rotation deformation of the basic roof contacts the gangue. When the numerical model runs to Fig. 6j, the rotation deformation of the basic roof contacts the goaf, and the basic roof reaches a stable state under the support of the gangue. This stage is called the second stage: the basic roof deformation stage. As shown in Fig. 6l–o, the basic roof reaches a stable state and no deformation occurs. The deformation coefficient of the final basic roof reaches 0.50, and the deformation degree of the basic roof is small. This stage is called the third stage: the basic roof stability stage.

Comparing the deformation movement of roof under the condition of NRDB and RDB, it can be seen that the

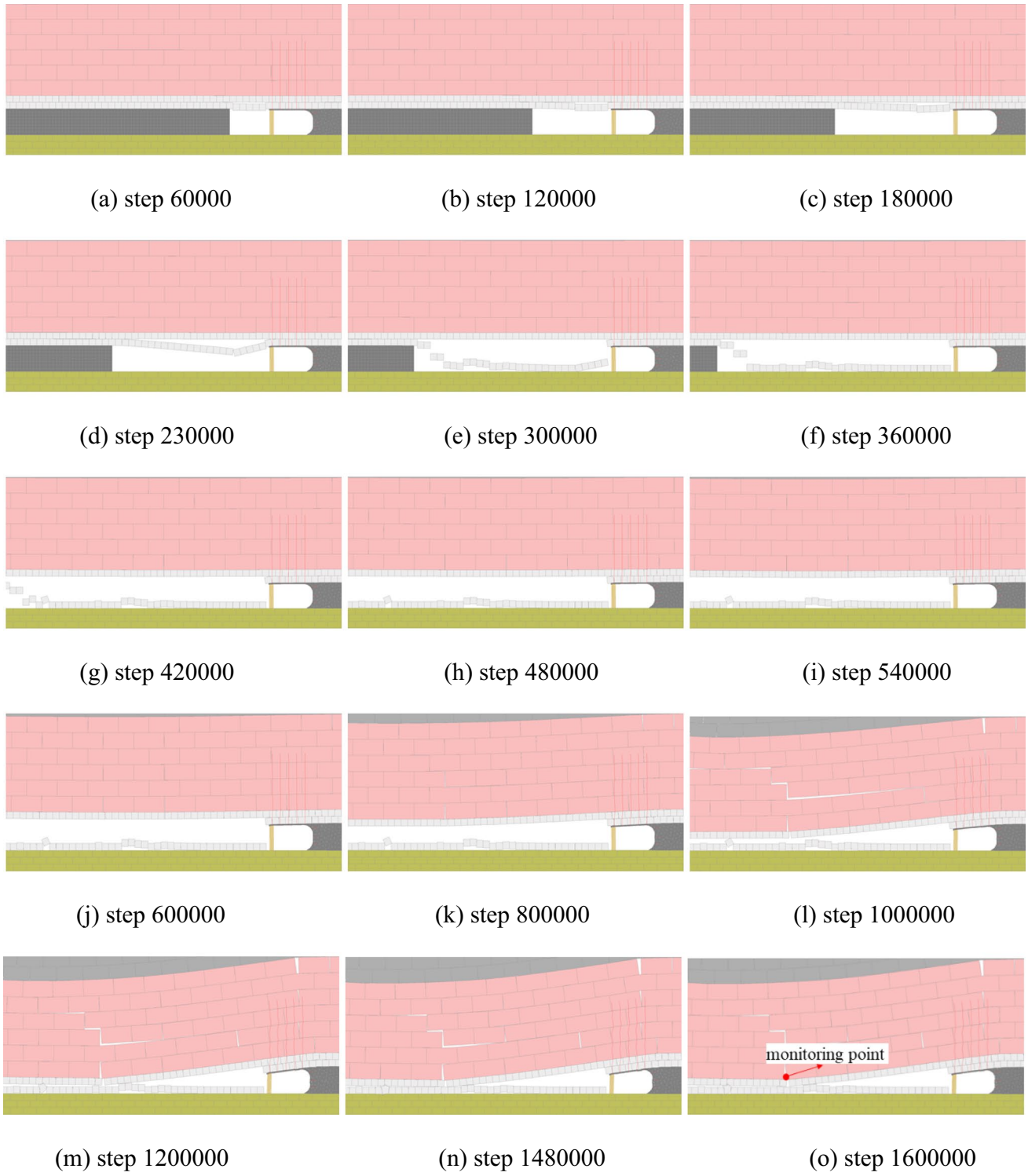

Fig. 5 Roof deformation process with the NRDB state

deformation movement of roof is divided into three stages. During the first stage, because the RDB cuts off part of the basic roof, the bearing capacity of the basic roof decreases in the RDB state. Under the action of overlying strata, the basic roof deforms first, as shown in Fig. 7. During the second stage, the deformation coefficient of the basic roof continues to increase in the RDB state. When the basic roof does not contact the gangue in the goaf, the bearing capacity of the

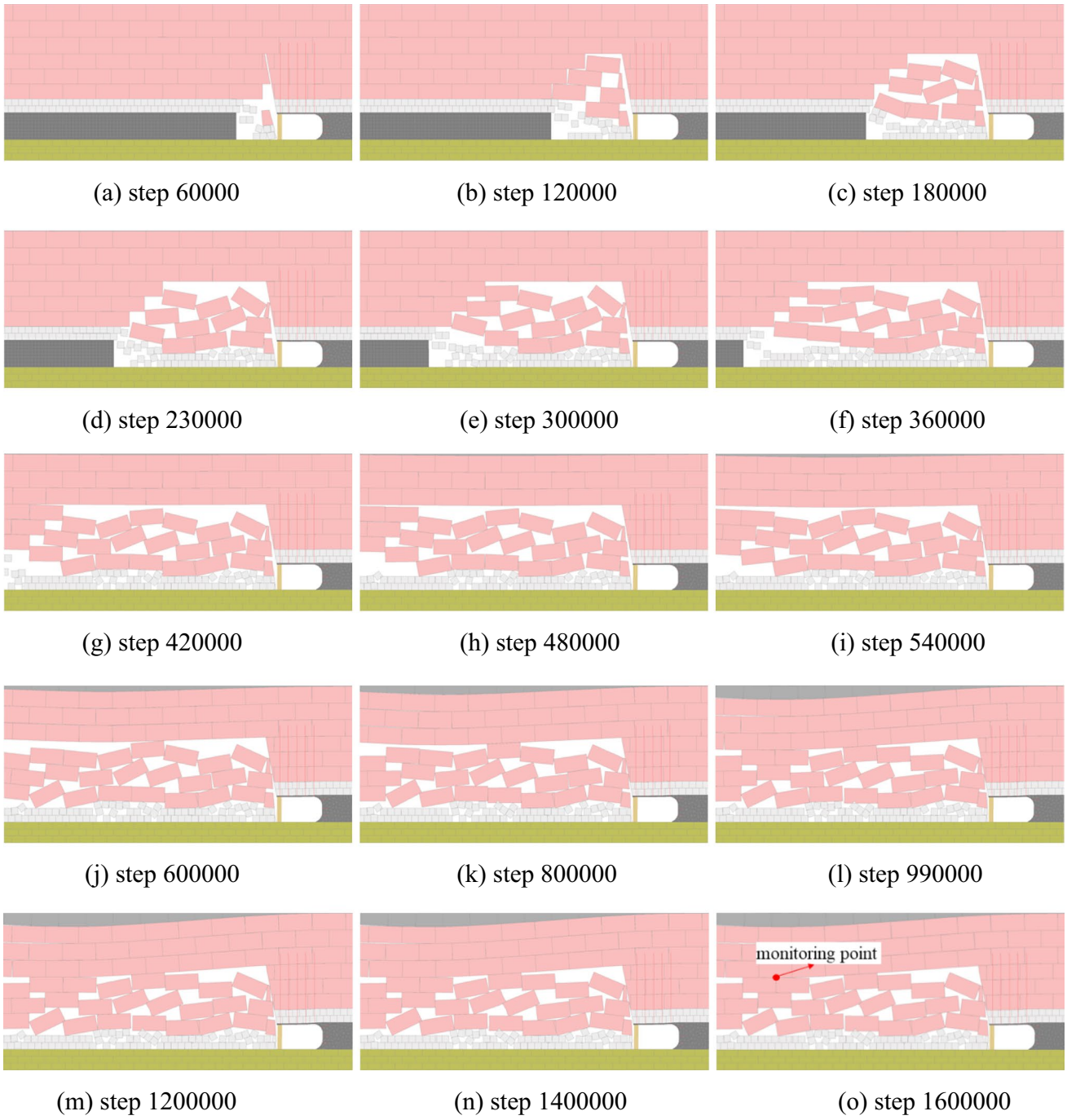

Fig. 6 Roof deformation process with the RDB state

basic roof is small. The deformation coefficient of the basic roof in the RDB state is larger than that in the NRDB state. After the basic roof touches the goaf in the RDB state, it is slowly stable under the support of the gangue, and the basic roof has not touched the goaf in the NRDB state. Therefore, after a period of contact with the goaf, the deformation coefficient of the basic roof in the RDB state is less than that in the NRDB state. The basic roof in the RDB state first reaches a stable state, and the deformation coefficient of the basic roof is less than that in the NRDB state. The stage that has the greatest impact on the deformation of basic roof is the basic roof deformation stage. The deformation coefficient of the basic roof in NRDB state is larger than that in RDB state. When the basic roof reaches a stable state, the steps of numerical model in NRDB state are greater than that in RDB state, which is mainly due to the influence of RDB.

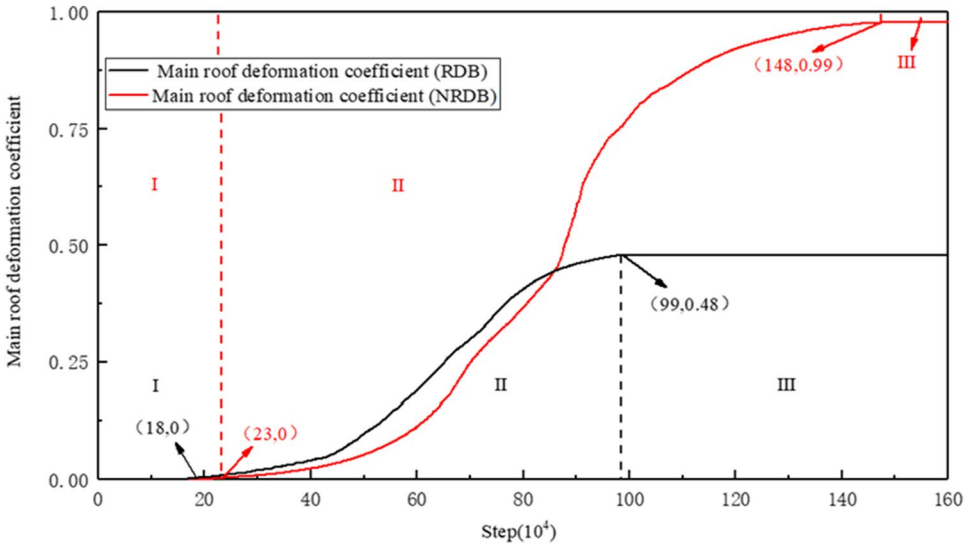

Fig. 7 Comparison of deformation coefficient data of basic roof under the RDB state and NRDB state

Part of the basic roof collapsed into the goaf to form gangue, the goaf is filled with the gangue and supports the basic roof, so that the basic roof in RDB state can reach a stable state faster and reduce its deformation degree.

4.2 Analysis of Roadway Deformation Evolution Law

To clarify the influence of roof deformation movement on roadway roof deformation in RDB, the deformation of roadway roof was monitored. The monitoring point was located in the middle of roadway roof, and the deformation and deformation velocity of roadway roof were analyzed.

In the NRDB state, as shown in Fig. 8, the deformation of the roadway roof in first stage is 15 mm due to the immediate roof collapse of the goaf. The deformation of the roadway roof in second stage is 586 mm due to the deformation of the basic roof, and the final deformation of roadway roof is 601 mm. In the RDB state, the roadway roof deformation in the first stage is 5 mm. Compared with the NRDB state, the roadway roof deformation decreases by 66.7% before the deformation of the basic roof. Whether the RDB state or NRDB state, the deformation of roadway roof during the first stage is very small. During the second stage, the deformation of roadway roof is 210 mm. Compared with the NRDB state, the deformation of roadway roof is reduced by 64.2%, and the final deformation of roadway roof reaches 215 mm. Compared with the NRDB state, the final deformation of roadway roof is reduced by 64.2%. Since then, it has entered the third stage. In this stage, the deformation is no longer generated, and the roof deformation is no longer changed. This is because the basic roof is supported by the gangue and reaches the equilibrium state. During the deformation process of the roadway roof, the deformation speed

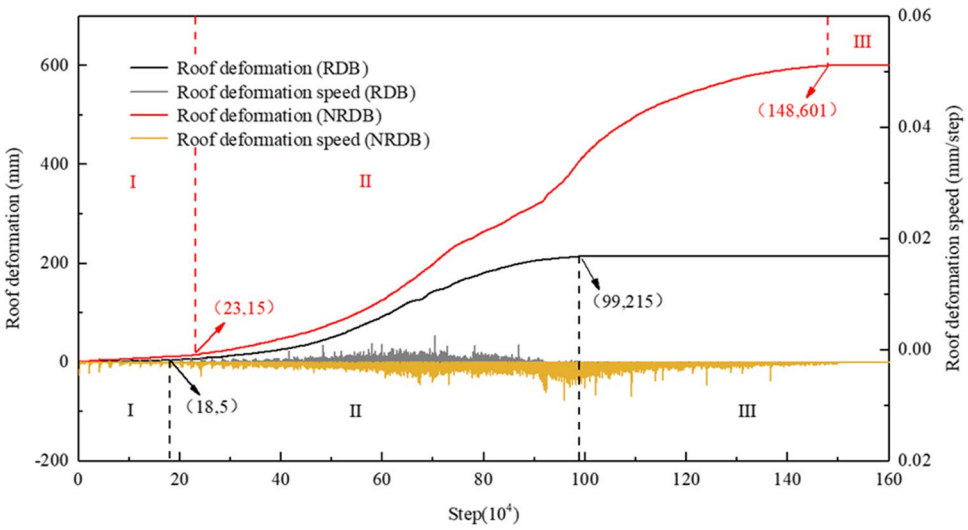

Fig. 8 Comparison of roadway roof deformation data under RDB state and NRDB state

of the roadway roof under the RDB state is less than that under the NRDB state.

The final deformation of roadway surrounding rock is shown in Fig. 9. As shown in Fig. 9a, the roadway roof and arc side are damaged under the NRDB state. At this time, the roadway can not meet the requirements of normal production, and there is a great potential safety hazard. The roof and arc side of roadway is intact in the RDB state. As shown in Fig. 9b, the deformation of roadway surrounding rock is small, and the basic roof has reached a stable state and meets the normal production requirements. This is because the RDB leads to the collapse of the immediate roof and part of the basic roof to the goaf during the mining. The goaf is filled with gangue. When the basic roof is rotated and deformed, it only needs a small rotation angle to contact the gangue, the basic roof is supported by the gangue and reaches a stable state.

4.3 Analysis of Roadway Stress Distribution Characteristics

To analyze the influence of RDB on the stress distribution characteristics of the arc side, the stress distribution of the arc side is monitored. In the monitoring process, it is found that the stress convergence is formed in the arc roadway side, and the position and size of the stress convergence are constantly changing during the operation of the whole model. In order to facilitate the analysis, the stress distribution characteristics under the final state are selected for analysis, which does no effect the analysis results. As shown in Fig. 10a, it shows the distribution characteristics of stress under the NRDB state. In the mining process, the stress redistribution, the peak value of stress convergence in the arc side reaches 10.7 MPa, and the maximum stress is 1.9 m away from the arc side. In the RDB state, as shown in Fig. 10b, the peak value of stress convergence in the arc side is 8.3 MPa, which is reduced by 22.4%. This is because the RDB makes some of the basic roof collapse in advance, the basic roof of the collapse forms gangue, which is full of goaf to a greater extent. The rotation deformation angle of the basic roof decreases and the stress convergence of the arc side is weakened. The maximum stress peak under RDB state is 3.1 m away from the arc side, and the distance increases by 63.2%. This is because the RDB blocks the stress transfer from the roof of some goaf to the side of the roadway and transfers the stress transfer path to the deep part of the arc side. In summary, the RDB changes the stress transfer path, weakens the stress convergence degree of the arc side, and improves the stability of the arc side.

5 Field Test Verification

5.1 Monitoring Method of Roadway Roof Deformation

In order to verify the accuracy of the numerical simulation, we carried out field tests and monitoring. Because the roadway may have safety problems such as large deformation and poor stability in the state of NRDB, it is difficult to carry out field tests. We only carried out field verification for the state of RDB. In the numerical simulation, the parameter

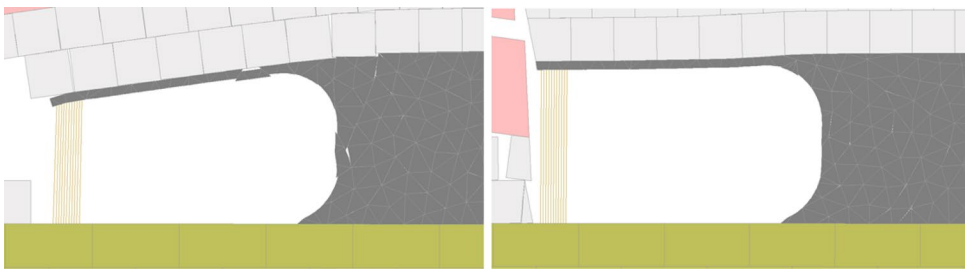

(a) NRDB state (b) RDB state

Fig. 9 Final deformation of roadway

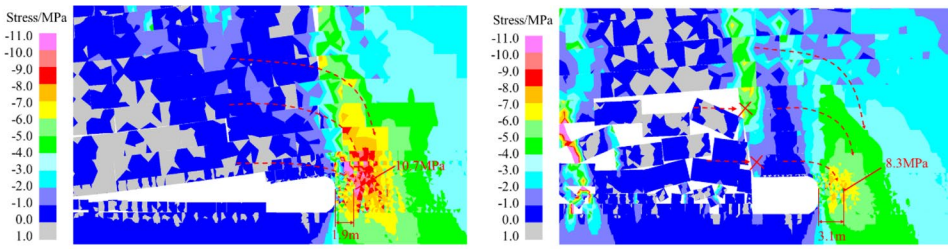

(a) NRDB state (b) RDB state

Fig. 10 Stress distribution of arc roadway under RDB state and NRDB state

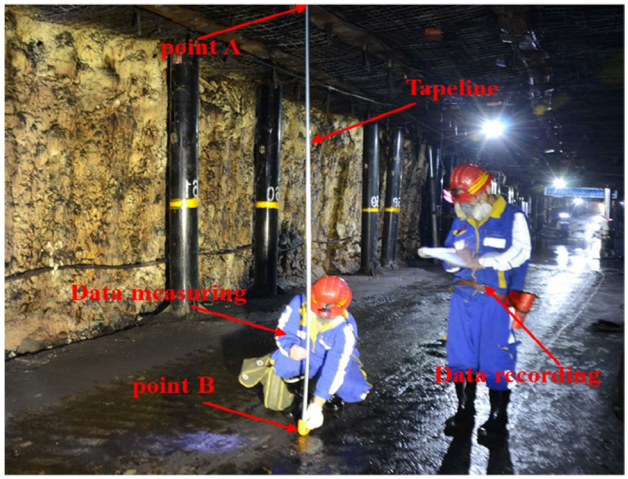

Fig. 11 Schematic diagram of on-site monitoring

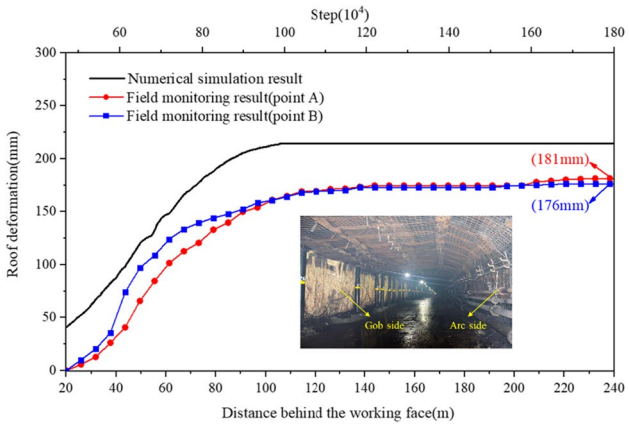

Fig. 12 Numerical simulation results and field monitoring results of roadway roof deformation

selection in the state of RDB and NRDB is consistent, so it is effective to only verify the state of RDB.

In the mining process of working face, in order to monitor the deformation of the roof of the roadway, a monitoring point is set every 20 m in the middle of the roadway. The data recording frequency of the monitoring point is once a day. There are two fixed personnel to monitor the data. As shown in Fig. 11, due to the influence of equipment construction near the working face, the data measurement of the field monitoring point is started from 20 m behind the working face. The RDB and roadway support at monitoring points have been completed. Because the working face has been mined a distance forward, there is some roof deformation data that cannot be monitored. However, this does not affect the use of field measurement data to verify the numerical simulation results.

5.2 Analysis of Monitoring Results

The field monitoring results and numerical simulation results are shown in Fig. 12. The deformation results of two monitoring points were selected for analysis, point A and point B. Due to the influence of the equipment in the roadway, the monitoring points are arranged at a distance behind the working face, and the immediate roof of the working face has collapsed before the layout of the monitoring point. The roadway roof has been affected by the collapse of the immediate roof, and a part of the displacement has been generated. Therefore, during the monitoring period, the deformation of the working face is mainly affected by the deformation of the basic roof. The roadway roof deformation increases rapidly in the range of 20–140 m behind the working face. After 220 m away from the working face, the deformation area of the roof is stable, indicating that the deformation of the basic roof is gradually reduced and stabilized after touching the gangue. At the same time, due to the broken expansion characteristic of rock, the goaf is filled with gangue. The deformation of the basic roof is small, and the final roof reaches a stable state. The final deformation of the two monitoring points is 181 mm and 176 mm respectively, with an average of 178.5 mm. The roadway state in the field is good, and the roadway roof remains stable. It can be seen from Fig. 12 that the field monitoring results are in good agreement with the numerical simulation results. In addition, the numerical simulation records the roof displacement data at the early stage of roadway formation, and this part of the data cannot be obtained in the process of field monitoring, which reflects the advantages of numerical simulation to a certain extent and can help us to obtain more comprehensive data, which is beneficial to the field engineering application.

6 Discussion

In this paper, the deformation movement of roof under RDB state and NRDB state are simulated by numerical simulation, which is divided into three stages. The deformation evolution law and stress distribution characteristics of roadway surrounding rock are analyzed. Through the field measured data, the results are consistent with the numerical simulation, which verifies the effectiveness of the numerical simulation.

Under the RDB state, the roof deformation movement is divided into three stages, which is the same as the theoretical research of many scholars. From their research theory, we can know that after the RDB, the roof strata in the range of RDB fall to the goaf to form gangue, which is full of goaf, as shown in Fig. 13a, this is consistent with the first stage: the goaf roof collapse stage (Fig. 6a–g). With the continuous deformation of the basic roof, the gangue is compacted, as shown in Fig. 13b, which is consistent with the second

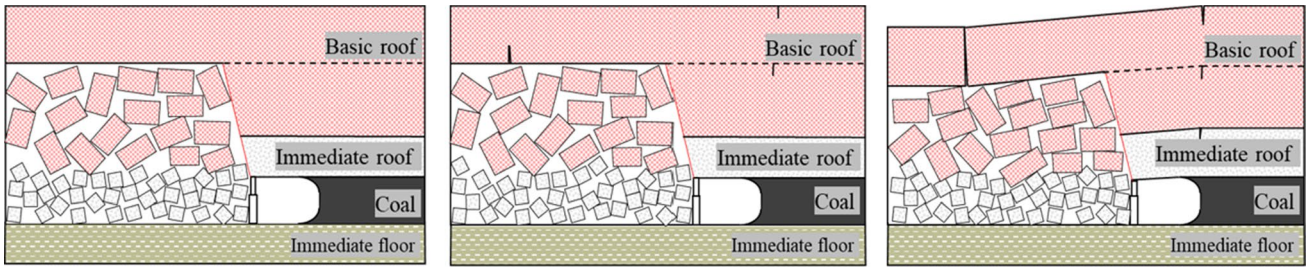

(a) the goaf roof collapse stage (b) the basic roof deformation stage (c) the basic roof stability stage

Fig. 13 Theoretical analysis model of roof deformation movement under RDB state

stage: the basic roof deformation stage (Fig. 6h–m). Finally, the basic roof reaches a stable state, as shown in Fig. 13c, which is consistent with the third stage: the basic roof stability stage (Fig. 6n–o). The results of this study are consistent with the theoretical analysis of other scholars [21], which further verifies the effectiveness of numerical simulation in theory.

It is not difficult to obtain from the results of this paper that the stability of roadway is mainly affected by the deformation of the basic roof. The basic roof deformation stage accounts for more than 97% of the total deformation of the roof. Therefore, it is essential to control the deformation of the basic roof. RDB is a very effective method. On the one hand, RDB causes more rock to collapse, and the goaf is filled with gangue, which supports the basic roof and reduces the deformation of the basic roof. On the other hand, RDB changes the stress transmission path of roof, weakens the peak stress convergence of arc side, and improves the stability of roadway.

At present, we have done experiments in shallow and medium-thick coal seams and achieved good results. For deep coal seams, we have not done more research. However, it is foreseeable that due to the increase of ground stress, the roadway bears greater stress, and the support of the roadway needs to be changed, which may increase the cost. Additionally, when GEFAWCP is applied in thin coal seam, it is also necessary to change the design of RDB according to the thickness of coal seam, such as the height of RDB, which is determined by mining height and bulking coefficient. In general, in the face of different mining conditions, GEFAWCP needs to make corresponding changes, which will be the focus of our future research.

7 Conclusion

(1) The numerical model of deformation movement of roof under the RDB state and NRDB state was established. The whole process of deformation movement of roof in the mining process was simulated. The characteristics of deformation movement of roof were analyzed. The deformation movement of roof was summarized into three stages: the goaf roof collapse stage, the basic roof deformation stage and the basic roof stability stage. The deformation coefficient of basic roof under the NRDB state was larger than that under the RDB state, and the continuous steps of the basic roof deformation stage were longer.

(2) The influence of roof movement at different stages on the deformation of roadway roof under the RDB state and the NRDB state is compared. Among them, the basic roof deformation stage has the greatest influence on roof deformation. Compared with the RDB state, the goaf is filled with gangue under the RDB state. When the basic roof is rotated and deformed, it only needs a small rotation angle to contact the gangue. The basic roof is supported by the gangue in the goaf and reaches a stable state. which reduces the deformation of roadway roof and improves the stability of roadway roof.

(3) The RDB can effectively improve the stress distribution of the arc side. The RDB cuts off the stress transfer path of some goafs roof, weakens the peak stress convergence on the arc side, and transfers the peak stress convergence to the deep part of the arc side, which improves the stability of the arc side.

Funding The authors acknowledge the financial support of the National Natural Science Foundation of China (Nos. 51904207, 52074164 and 42077267), China Postdoctoral Science Foundation (No.2019M661622), the State Key Laboratory for Geomechanics and Deep Underground Engineering Shanxi Yinfeng Branch Center Foundation (No. YFKT-202002), the State Key Laboratory for Geomechanics and Deep Underground Engineering, China University of Mining & Technology/China University of Mining & Technology, Beijing (No. SKLGDUEK2131), and the Institute for Deep Underground Science and Engineering, China University of Mining & Technology, Beijing (No. XD2021023).

Data Availability Some or all data during the study are available from the corresponding author by request.

Declarations

Conflict of Interest The authors declare no competing interests.

References

1. Emery J, Canbulat I, Craig P, Naylor J, Sykes A (2016) Development and implementation of spin to stall resin at Anglo Americans Australian underground coal operations. Int J Min Sci Techno 26:161–168. https://doi.org/10.1016/j.ijmst.2015.11.025
2. Peng SS, Du F, Cheng JY, Li Y (2019) Automation in U.S. longwall coal mining: a state-of-the-art review. Int J Min Sci Techno 29:151–159. https://doi.org/10.1016/j.ijmst.2019.01.005
3. Sears MM, Esterhuizen GS, Tulu IB (2019) Overview of current us longwall gateroad support practices: an update. Mining Metall Explor 36:1137–1144. https://doi.org/10.1007/s42461-019-0077-3
4. Alber M, Fritschen R, Bischoff M, Meier T (2009) Rock mechanical investigations of seismic events in a deep longwall coal mine. Int J Rock Mech Min 46:408–420. https://doi.org/10.1016/j.ijrmms.2008.07.014
5. Jiang HJ, Cao SG, Zhang Y, Wang C (2016) Analytical solutions of hard roof's bending moment, deflection and energy under the front abutment pressure before periodic weighting. Int J Min Sci Techno 26:175–181. https://doi.org/10.1016/j.ijmst.2015.11.027
6. Zhang B, Cao SG (2015) Study on first caving fracture mechanism of overlying roof rock in steep thick coal seam. Int J Min Sci Techno 25:133–138. https://doi.org/10.1016/j.ijmst.2014.11.013
7. Zou QL, Liu H, Zhang YJ, Li QM, Fu JW, Hu QT (2020) Rationality evaluation of production deployment of outburst-prone coal mines: a case study of nantong coal mine in Chongqing. Saf Sci 122:e104515. https://doi.org/10.1016/j.ssci.2019.104515
8. Wang Q, Pan R, Jiang B, Li SC, He MC, Sun HB et al (2017) Study on failure mechanism of roadway with soft rock in deep coal mine and confined concrete support system. Eng Fail Anal 81:155–177. https://doi.org/10.1016/j.engfailanal.2017.08.003
9. Wang Q, Gao HK, Jiang B, Li SC, He MC, Qin Q (2021) In-situ test and bolt-grouting design evaluation method of underground engineering based on digital drilling. Int J Rock Mech Min 138:e104575. https://doi.org/10.1016/j.ijrmms.2020.104575
10. Lu J, Hasenfus G (2019) Challenges of mining the first right-handed longwall panel in a new reserve block in pittsburgh seam. Int J Min Sci Techno 29:145–149. https://doi.org/10.1016/j.ijmst.2018.11.010
11. Li WF, Bai JB, Peng S, Wang XY, Xu Y (2015) Numerical modeling for yield pillar design: a case study. Rock Mech Rock Eng 48:305–318. https://doi.org/10.1007/s00603-013-0539-8
12. Guo PF, Yuan YD, Ye KK, Sun DJ (2021) Fracturing mechanisms and deformation characteristics of rock surrounding the gate during gob-side entry retention through roof pre-fracturing. Int J Rock Mech Min 148:e104927. https://doi.org/10.1016/j.ijrmms.2021.104927
13. Wang HS, Zhang DS, Fan GW (2011) Structural effect of a soft–hard backfill wall in a gob-side roadway. Min Sci Tech 21:313–318. https://doi.org/10.1016/j.mstc.2011.05.001
14. Ma ZG, Gong P, Fan JQ, Geng MM, Zhang GW (2011) Coupling mechanism of roof and supporting wall in gob-side entry retaining in fully-mechanized mining with gangue backfilling. Min Sci Tech 21:829–833. https://doi.org/10.1016/j.mstc.2011.05.036
15. Deng YH, Tan JX, Zhu XK, Fu Y, Dai ZY (2010) Analysis and application in controlling surrounding rock of support reinforced roadway in gob-side entry with fully mechanized mining. Min Sci Tech 20:839–845. https://doi.org/10.1016/S1674-5264(09)60292-1
16. He MC, Zhu GL, Guo ZB (2015) Longwall mining "cutting cantilever beam theory" and 110 mining method in China - the third mining science innovation. J Rock Mech Geotech Eng 7:483–492. https://doi.org/10.1016/j.jrmge.2015.07.002
17. He MC, Gao YB, Yang J, Gong WL (2017) An innovative approach for gob-side entry retaining in thick coal seam longwall mining. Energies 10:e1785 (https://doi-org-s.vpn.cumtb.edu.cn:8118/10.3390/en10111785)
18. Wang Q, Wang Y, He MC, Jiang B, Li SC, Jiang ZH et al (2021) Experimental research and application of automatically formed roadway without advance tunneling. Tunn Undergr Space Technol 114:103999. https://doi.org/10.1016/j.tust.2021.103999
19. Wang Q, He MC, Yang J, Gao HK, Jiang B, Yu HC (2018) Study of a no-pillar mining technique with automatically formed gob-side entry retaining for longwall mining in coal mines. Int J Rock Mech Min 110:1–8. https://doi.org/10.1016/j.ijrmms.2018.07.005
20. Yang J, Wang HY, Wang YJ, Gao YB, Wang JW, Hui L (2019) Fracture characteristics of the roof in gob-side entry retaining with roof cutting and pressure release. J Min Saf 36:1137–1144. https://doi.org/10.13545/j.cnki.jmse.2019.06.009
21. Yang J, Fu Q, Gao YB, Cheng Y, Zhang JB (2020) Research on roof deformation laws and mechanism in a non-pillar mining method with entry automatically formed during the whole cycle. J China Coal Soc 45:87–98. https://doi.org/10.13225/j.cnki.jccs.2019.1625
22. Yang J, He MC, Cao C (2019) Design principles and key technologies of gob side entry retaining by roof pre-fracturing. Tunn Undergr Space Technol 90:309–318. https://doi.org/10.1016/j.tust.2019.05.013
23. Wang YJ, Wang Q, He MC, Hou SL, Yang J, Gao YB (2021) Stress and deformation evolution characteristics of gob-side entry retained by the N00 mining method. Geomech Geophys Geo 7:1–18. https://doi.org/10.1007/s40948-021-00279-w
24. Gao YB, Yang J, Wang Q, Wang YJ, He MC (2017) Mechanism of roof presplitting in a nonpillar mining method with entry automatically retained and its influence on the strata behaviors. J China Coal Soc 44:3349–3359. https://doi.org/10.13225/j.cnki.jccs.2019.0652
25. Liu JN, He MC, Wang YJ, Huang RF, Yang J, Tian XC et al (2019) Stability analysis and monitoring method for the key block structure of the basic roof of noncoal pillar mining with automatically formed gob-side entry. Adv Civ Eng 8:1–14. https://doi.org/10.1155/2019/5347683
26. Liu JN, He MC, Hou SL, Zhu Z, Wang YJ, Yang J (2021) Force change of the gravel side support during gangue heaping under a new non-pillar-mining approach. Geomech Eng 27:31–43. https://doi.org/10.12989/gae.2021.27.1.031
27. Yang XJ, Wang EY, Ma XG, Zhang GF, Huang RF, Lou HP (2019) A case study on optimization and control techniques for entry stability in non-pillar longwall mining. Energies 12:e391. https://doi.org/10.3390/en12030391
28. Zhang XY, Hu JZ, Xue HJ, Mao WB, Gao YB, Yang J et al (2020) Innovative approach based on roof cutting by energy-gathering blasting for protecting roadways in coal mines. Tunn Undergr Space Technol 99:e103387. https://doi.org/10.1016/j.tust.2020.103387
29. Zhang XY, Pak RYS, Gao YB, Liu CK, Zhang C, Yang J et al (2020) Field experiment on directional roof presplitting for pressure relief of retained roadways. Int J Rock Mech Min 134:e104436. https://doi.org/10.1016/j.tust.2020.103387
30. Zhang Q, He MC, Wang J, Guo S, Guo ZB, Liu XY et al (2020) Instantaneous expansion with a single fracture: a new directional rock-breaking technology for roof cutting. Int J Rock Mech Min 132:1365–1609. https://doi.org/10.1016/j.ijrmms.2020.104399
31. Zhang Q, He MC, Guo S, Qi JC, Yang J, Wang C, Xia M, Li LN (2022) Investigation on the key techniques and application of the

new-generation automatically formed roadway without coal pillars by roof cutting. Int J Min Sci Techno 152:1365–1609. https://doi.org/10.1016/j.ijrmms.2022.105058
32. Meng FF, Pu H, Sasaoka T, Shimada H, Liu S, Dintwe TKM et al (2021) Time effect and prediction of broken rock bulking coefficient on the base of particle discrete element method. Int J Min Sci Techno 31:643–651. https://doi.org/10.1016/j.ijmst.2021.05.004
33. Zhang LY, Einstein HH (2004) Using RQD to estimate the deformation modulus of rock masses. Int J Rock Mech Min 41:337–341. https://doi.org/10.1016/S1365-1609(03)00100-X
34. Gao F, Stead D (2014) The application of a modified Voronoi logic to brittle fracture modelling at the laboratory and field scale. Int J Rock Mech Min 68:1–14. https://doi.org/10.1016/j.ijrmms.2014.02.003
35. Singh M, Rao KS (2005) Empirical methods to estimate the strength of jointed rock masses. Eng Geol 77:127–137. https://doi.org/10.1016/j.enggeo.2004.09.001
36. Wilson AH (1984) The stability of underground workings in the soft rocks of the coal measures. Int J Rock Mech Min 1:91–187. https://doi.org/10.1016/0148-9062(84)90114-1
37. Hoek E, Brown ET (1997) Practical estimates of rock mass strength. Int J Rock Mech Min Sci 34:1165–1186. https://doi.org/10.1016/S1365-1609(97)80069-X
38. Brady BHG, Brown ET (2006) Rock mechanics for underground mining. Springer, Dordrecht. https://books.google.co.jp/books?hl=zh-CN&lr=&id=WiVNf9h4_VIC&oi=fnd&pg=PR11&ots=Y1Hhb6frVM&sig=kVq0ncoFXFea_a1n8K0Sn6F_U4&redir_esc=y#v=onepage&q&f=false